

The role of soil-surface sealing, microtopography, and vegetation patches in rainfall-runoff processes in semiarid areas

L. Chen,¹ S. Sela,² T. Svoray,² and S. Assouline³

Received 16 December 2012; revised 10 June 2013; accepted 11 June 2013; published 13 September 2013.

[1] The hydrological response of semiarid watersheds to short but intense rainfall events is complex due to feedbacks among water fluxes, vegetation patches, topography, and soil properties. This paper seeks to quantify the combined impact of soil-surface sealing, microtopography, and vegetation patches on surface hydrologic processes on a semiarid hillslope. A modeling approach using a two-layer conceptual infiltration model and two-dimensional surface runoff model was developed to study rainfall-runoff relationships. This combined model is applicable to heterogeneous areas with spatially varying soil properties, landscape, and land-cover characteristics. Data from a semiarid site in southern Israel was used to evaluate the model and analyze fundamental hydrologic mechanisms. Our results indicate that seal layer, microtopography, and vegetation play important roles in dry land runoff processes: seal layer controls runoff generation; vegetation patches affect overland flow by enhancing local infiltration rates; microtopography has a small impact on the total amount of runoff, but shapes the spatial pattern of overland flow. The presence of vegetation patches amplifies the effect of microtopography by increasing spatial variability of infiltration and runoff. Results also show that water resource allocation favors vegetation patches through surface runoff, with maximum local cumulative infiltration one order of magnitude higher than the amount of water available from rainfall. This suggests a sophisticated system of water resource distribution in semiarid ecosystems through complex interactions among environmental factors.

Citation: Chen, L., S. Sela, T. Svoray, and S. Assouline (2013), The role of soil-surface sealing, microtopography, and vegetation patches in rainfall-runoff processes in semiarid areas, *Water Resour. Res.*, 49, 5585–5599, doi:10.1002/wrcr.20360.

1. Introduction

[2] The partitioning of rainfall into infiltration and runoff at the soil surface is of particular importance in semiarid environments. Runoff processes can change dramatically the allocation of water resources, supplying plants with water from remote areas [Kirkby and Chorley, 1967; Descroix et al., 2007; Lehmann et al., 2007; Thompson et al., 2010a, 2010b]. Hortonian (infiltration excess) runoff is one of the major runoff-generation mechanisms in these environments [Lange and Leibundgut, 2003; Wainwright and Bracken, 2011], especially under short but intensive rainfall events. Infiltration and overland flow, as the two major components of the hydrological response, are dynamically coupled in space and time, as well as shaped

by both rainfall and surface characteristics. Among surface characteristics affecting dry land hydrology, three are most commonly observed: (a) presence of a seal layer at the soil surface; (b) surface microtopography; and (c) vegetation patches.

[3] The seal layer developing at the vicinity of a bare soil surface is a more compacted and, therefore, less permeable layer—reducing infiltration [e.g., Hillel and Gardner, 1969, 1970; Ahuja, 1974; Mualem and Assouline, 1989; Abu-Awwad, 1997; Assouline and Mualem, 1997; Vandervaere et al., 1998; Assouline, 2002, 2004; Carmi and Berliner, 2008; Davis et al., 2010]. The seal layer also was found to affect substantially water-content dynamics and evaporation from the soil [Bresler and Kemper, 1970; Sela et al., 2012]. Although biological crusts also are often present on dryland surfaces [e.g., Belnap, 1990; Kidron et al., 2012], our focus in this paper is on mechanical sealing of the soil surface. This seal layer is the outcome of either (a) raindrops impinging and sudden wetting of soil aggregates (structural seals) or (b) settling of fine particles (depositional seals) [Assouline, 2004]. In both cases, it drastically reduces soil hydraulic conductivity and therefore enhances runoff generation [Mualem and Assouline, 1989; Assouline and Mualem, 2006]. Although soil-surface sealing is a major factor in dryland hydrology, it rarely has been included in modeling studies and its role, as a water allocation mechanism, needs further investigation.

¹Division of Hydrologic Sciences, Desert Research Institute, Las Vegas, Nevada, USA.

²Department of Geography and Environmental Development, Ben-Gurion University of the Negev, Beer Sheva, Israel.

³Department of Environmental Physics and Irrigation, Institute of Soil, Water and Environmental Sciences, A.R.O.–Volcani Center, Bet Dagan, Israel.

Corresponding author: L. Chen, Division of Hydrologic Sciences, Desert Research Institute, Las Vegas, NV 89119, USA. (lchen@dri.edu)

[4] Topography has been found to affect both infiltration rate [Zaslavsky and Sinai, 1981] and runoff generation [Mayor et al., 2008]. At the hillslope scale, opposite trends were reported regarding the effect of slope steepness on infiltration, depending on the soil and slope conditions that are considered [Philip, 1991; Chen and Young, 2006; Essig et al., 2009; Ribolzi et al., 2011]. At the basin scale, the channel network, as the major topographic feature, provides rapid pathways for runoff and dominates the routing process.

[5] At the local scale, microtopography produces non-uniform runoff patterns—segregating flow into narrow, relatively deep and fast-flow zones where velocity can be 2–7 times higher than the average flow as well as broader, shallower, slower-moving zones where velocity may approach zero [Dunkerley, 2003, 2004; Römkens et al., 1986]. Theoretical estimates [Thompson et al., 2010a, 2010b] showed that, with the effects of slope and local depressions, microtopography can increase rainfall infiltration by more than 20%, compared with the flat, planar slope case in which microtopography is absent. Microtopography has been included in previous modeling studies aimed to investigate its overall impact on runoff [Tayfur et al., 1993; Helmers and Eisenhauer, 2006; Appels et al., 2011], but its impact on spatial variability of the rainfall-runoff process requires further investigation.

[6] As an essential element of the dryland landscape, vegetation is one of the main factors determining hydrologic response—fluencing evapotranspiration, infiltration, and runoff routing [Abrahams et al., 1995; Ivanov et al., 2008a, 2008b, 2010; Peel, 2009; Seneviratne et al., 2010]. Most studies found vegetation patches to reduce runoff and sediment yield [Dunne et al., 1991; Reid et al., 1999; Muñoz-Robles et al., 2011], although opposite results also were reported [e.g., Cantón et al., 2011]. At the patch scale, vegetation plays various roles in the rainfall-runoff process. One option is that vegetation increases surface roughness, which changes the flow-routing pattern and erosion processes. Alternatively, vegetation affects infiltration by changing hydraulic properties of the underneath and surrounding soil [Thompson et al., 2010a, 2010b]. Most studies found vegetation to greatly increase soil hydraulic conductivity from bare soil interspace to under canopy, reporting up to 3–5 times higher infiltration under vegetation [Bromley et al., 1997; Dunkerley, 2000; Titus et al., 2002; Bhark and Small, 2003]. However, opposite results also were reported for soils characterized by relatively high saturated hydraulic conductivity ($>20 \text{ cm h}^{-1}$) [Caldwell et al., 2008].

[7] Modeling is an effective way to explore the complex interaction among infiltration, overland flow, and the several impacting factors involved. To study the dynamics of rainfall-runoff processes, mechanistic modeling approaches were developed based on infiltration theory, shallow water equations, and their simplified versions [Zhang and Cundy, 1989; Tayfur et al., 1993; Liu et al., 2004]. In these approaches, infiltration can be simulated by Richards' equation or simplified infiltration models such as Green and Ampt [1911], Philip [1957], and Smith and Parlange [1978] [see Assouline, 2013]. Runoff can be simulated by the St. Venant (full dynamic wave) equations or approximations mainly including kinematic wave and diffusion

wave equations [Singh, 1996]. Spatial and temporal variation of runoff and infiltration are naturally addressed when numerical techniques are used to solve the governing equations. In these approaches, either one-dimensional (1-D) or two-dimensional (2-D) spatial discretization of the modeling domain allows incorporation of heterogeneous surface features, with 2-D approaches providing more detailed representation.

[8] Previous studies have examined the impact of the sealing layer, microtopography, and vegetation as individual factors on rainfall-runoff partitioning. Their roles are not fully understood however, when all these attributes come into play together, which is often the case in natural environments. These factors may change the spatiotemporal coupling of infiltration and runoff and alter the water resources distribution mechanisms. Our aim is to gain better understanding of rainfall-runoff dynamics in semiarid environments and to unearth the contributing role of each of the aforementioned factors, as well as their mutual interactions in this complex system. For our purpose, we developed a suitable model to account for all essential impacting factors and applied this model to examine fundamental mechanisms underlying the system.

2. Study Site

2.1. The Site and The Runoff Plot

[9] The study site (Figure 1) is located at the Long Term Ecological Research (LTER) Lehavim site ($31^{\circ}20'N$, $34^{\circ}45'E$) in the semiarid area of the Northern Negev, Israel. Mean annual rainfall is 290 mm, occurring mostly from November to March. The dominant rock formations are Eocene limestone and chalk with patches of calcrete. Soils are brown lithosols and arid brown loess, prone to surface sealing. The dominant vegetation species is *Sarcopoterium spinosum* (a dwarf shrub), surrounded by patches of annual herbaceous vegetation [Svoray and Karnieli, 2011].

[10] Our objective was to obtain in-depth understanding of the runoff generation mechanism and water resources distribution in this semiarid landscape. We conducted extensive field surveys to enable detailed reconstruction with geographic information systems (GIS) of a historical field runoff plot ($18.8 \times 4 \text{ m}$). This plot was used previously [Kossovsky, 1994; Yair and Kossovsky, 2002] to conduct field runoff measurements under natural rainfall conditions. The rainfall and runoff data used in this study are from two rainstorm events in the 1991–1992 rain season, published by Kossovsky [1994]. The first storm, denoted hereafter as storm 1, occurred during four consecutive days (31 December 1991 to 3 January 1992) and resulted in total rain depth of 51.3 mm. The second storm, denoted hereafter as storm 2, occurred within two days (25–26 February 1992) and resulted in total rain depth of 32.6 mm. Maximum intensity measured for the two storms was 39 mm h^{-1} and 16 mm h^{-1} for storms 1 and 2, respectively. Frequency analysis shows that these two storms have a 100% annual exceedance of probability (or reoccur annually) for maximum 15, 30, and 60 min rainfall depths, and a 60% and 70% annual exceedance of probability for 24 h depth for storms 1 and 2, respectively, or about a 1.5 year recurrence interval for both storms. These frequencies

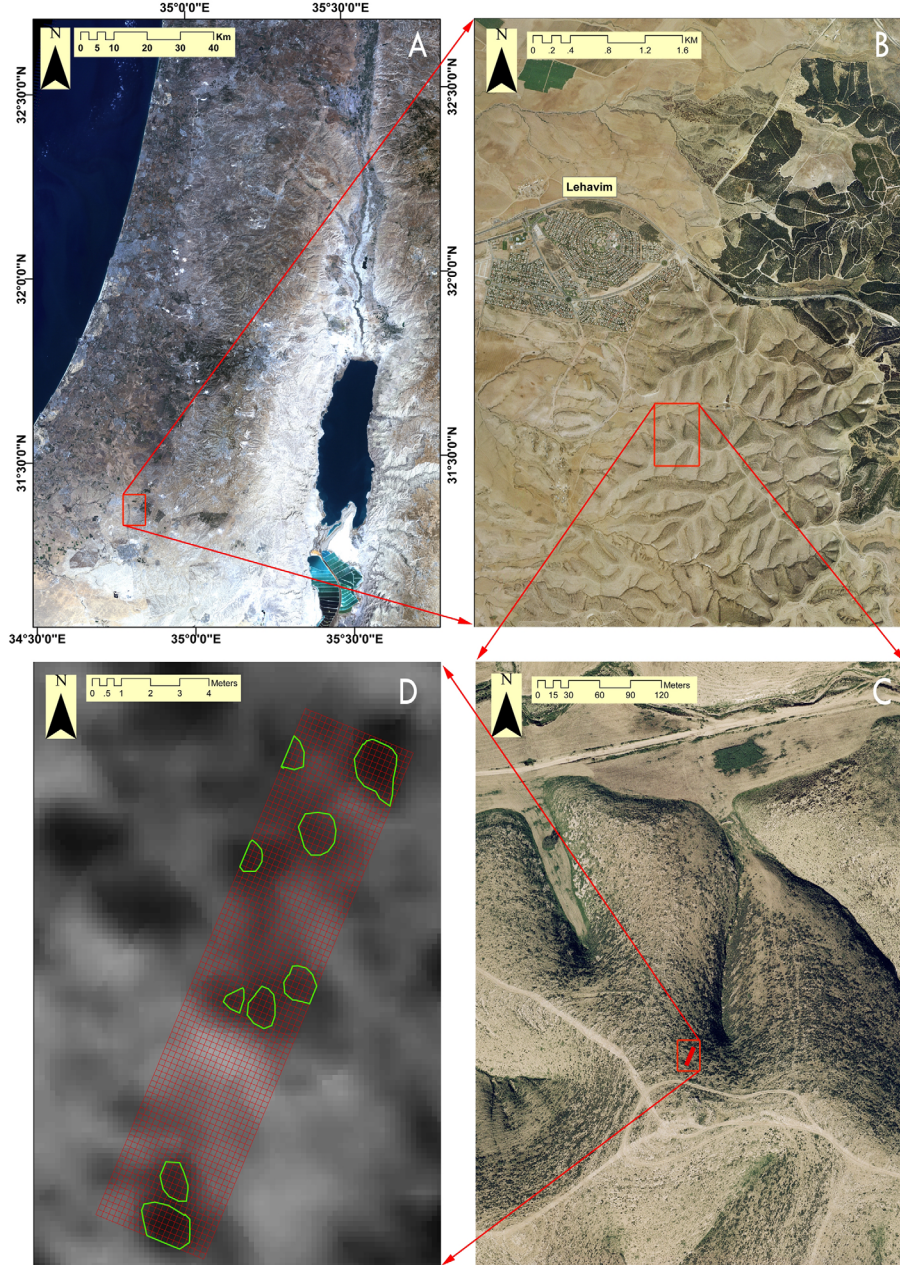


Figure 1. The field site at LTER and the runoff plot 11A (Figure d). In Figure 1d, the arrow indicates the flow direction, the mesh defines the runoff plot and computational grid, and the polygons represent vegetation patches.

suggest that results derived from these storms will be applicable to a wide range of rainfall conditions, rather than only extreme events, at the study site.

2.2. Topographic, Soil, and Vegetation Data

[11] All surface features—including microtopography, soil hydraulic properties, and vegetation distribution—were obtained through field sampling or remote sensing image analysis. Figure 2 depicts these main features of the plot.

2.2.1. Digital Elevation Model

[12] The digital elevation model (DEM) is a base layer used to extract other topographic information. The effect of the DEM grid size and integrity on hydrologic simulations was highlighted extensively previously [e.g., Zhang and

Montgomery, 1994; Erskine et al., 2007]. To obtain a high-resolution DEM, 150 elevation measurements (~ 0.5 m intervals) were made at the intershrub areas of the runoff plot using an electronic theodolite (SOKIA Inc. Total Station). These point measurements were interpolated using ordinary kriging (RMSE = 0.05 m) to produce a 5 cm horizontal resolution DEM data set as a base GIS layer (ESRI ArcGIS 9.3.1).

2.2.2. Shrubs and Rock Outcrops

[13] To account explicitly for distribution of vegetation patches that appeared when runoff measurements were made, we used a historic aerial image of the study site dated 4 September 1992. From this image, shrub locations were manually digitized and validated against visual

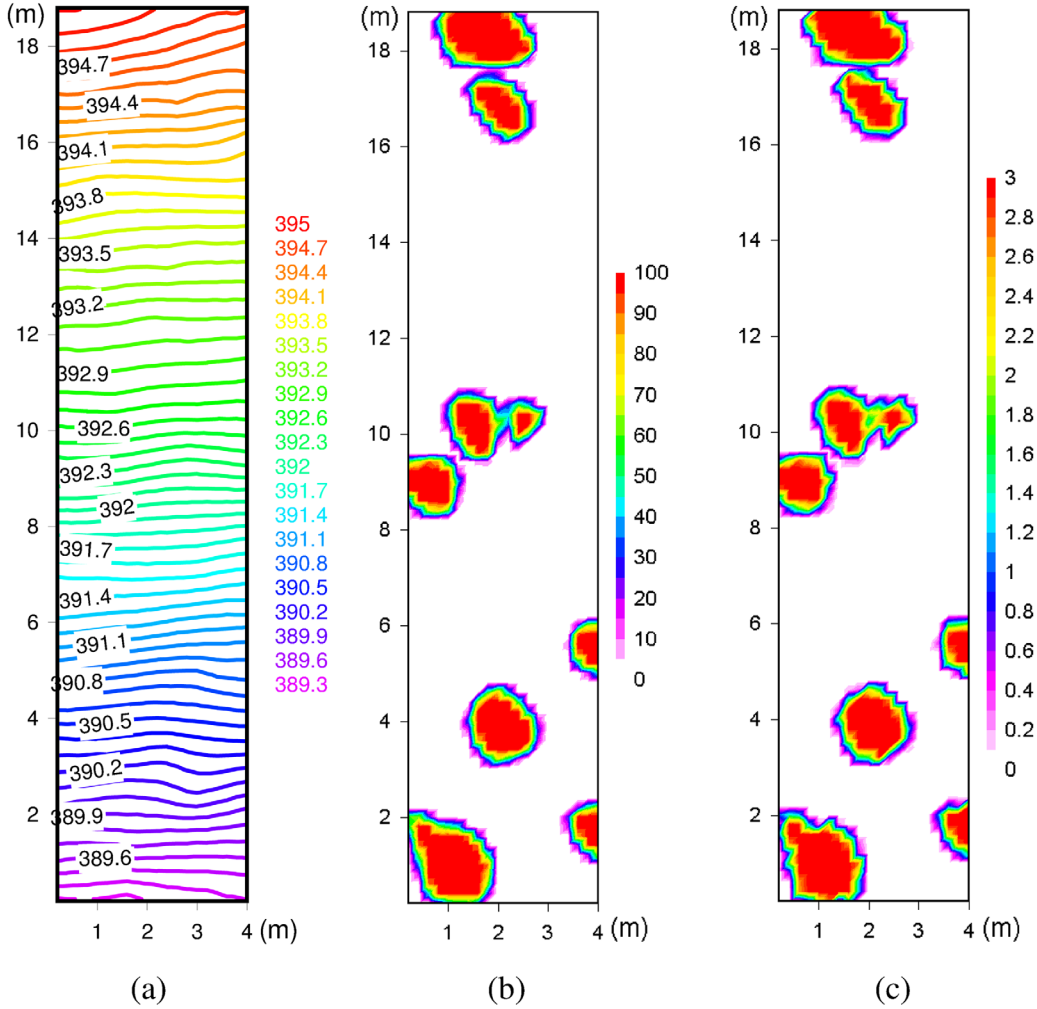


Figure 2. Characteristics of the field plot: (a) Topography (m); (b) percent shrub coverage (%); and (c) saturated hydraulic conductivity of the top soil (cm h^{-1}). Flow is from up to down.

interpretation. To account for rock outcrops, a higher resolution ($10 \times 10 \text{ cm}^2$) aerial orthophoto dated 31 December 2010 was used since we assumed that changes in rock outcrops during the past two decades were negligible. On this photo, maximum likelihood classification (MLC) [Svoray *et al.*, 2008] was used to extract outcrop locations.

2.2.3. Soil and Seal Layers Parameters

[14] The hydraulic properties of the seal layer were calculated following the model of Mualem and Assouline [1989], using parameters of the underlying undisturbed soil as input. A detailed description of the soil hydraulic parameters used for the simulations and methods used can be found in Sela *et al.* [2012]. In short, the water retention curve parameters used for the simulations corresponded to a reference curve for a Loess-type soil with a bulk density of 1.48 g cm^{-3} , as presented in Mualem and Assouline [1989]. This reference water retention curve was corrected for actual soil bulk density, ρ , at the site, following the approach in Assouline [2006] and using the relationships:

$$\alpha_v = 0.0078 \left(\frac{\rho}{1.48} \right)^{-3.72} \quad (1)$$

$$n = (3.733\rho - 3.644)^{0.845} \quad (2)$$

$$\theta_r = 0.04 \frac{\rho}{1.48} \quad (3)$$

where α_v and n are [van Genuchten, 1980] soil hydraulic parameters and θ_r is the residual soil water content. The soil bulk density ρ is related to the soil porosity Φ , using the following equation, assuming soil particle density $\rho_s = 2.65 \text{ g cm}^{-3}$:

$$\rho = \rho_s(1 - \Phi) \quad (4)$$

[15] The bulk density was estimated using the relationships in Saxton *et al.* [1986], based on the fraction of sand, silt, and clay in soil sampled at the site. Finally, the saturated water content of the soil (θ_s) was assumed to be equal to soil porosity Φ .

[16] The saturated hydraulic conductivity of the undisturbed parent soil for the Lehavim LTER site was estimated following Sela *et al.* [2012] by:

$$K_s = 5.58 - 0.11(\% \text{clay}) (\text{cm h}^{-1}) \quad (5)$$

where (%clay) represent the relative part of the clay component in the soil mechanical analysis. Seal-layer conductivity was estimated to be 0.019 cm h^{-1} according to calibration of an infiltration model carried out by Mualem *et al.* [1993] on data from infiltration experiments on Loess soil performed by Benyaminini [1981]. See Appendix A.1 for the soil hydraulic parameters used in the modeling study.

[17] Reports regarding the influence of shrubs on saturated hydraulic conductivity of adjacent soil via lateral root distribution and improvement of soil conditions can be found in the literature [e.g., Bhark and Small, 2003]. This effect is greatly limited for the dominant shrub species of the study site (*Sarcopoterium spinosum*), which was found to have mainly a vertical root system, capable of using water stored within deeper bedrock fissures [Henkin *et al.*, 1998]. This is further supported by field observation of the presence of sealed soil immediately following the edge of the shrub canopy, suggesting a sharp contrast in infiltration. Therefore, the shrubs' effect on saturated hydraulic conductivity of the surrounding soil beyond its crown was assumed to be negligible. The effect of the *Sarcopoterium spinosum* shrub on improved infiltration rates of the soil directly below its crown, relatively to the surrounding soil, was studied previously at the site indirectly [Kossovsky, 1994; Yair and Kossovsky, 2002; Segoli *et al.*, 2008]. In these studies, shrubs were found to enhance infiltration and reduce runoff substantially. To the best of our knowledge, however, no saturated hydraulic conductivity value for the soil under the shrubs at the site has been published. Therefore, since the crown canopy shelters the soil from the impact of raindrops and prevents formation of a surface seal which reduces infiltration into the soil, we used a saturated hydraulic conductivity value of 3 cm h^{-1} , representing the average value of the undisturbed soil of the intershrub areas in the study site, for the soil under every shrub canopy crown. This value reflects a sharp ratio of 1:157 between the saturated hydraulic conductivity of the seal layer and the soil under the shrub canopy crown.

3. Modeling Approach

[18] The aim of this study is to investigate the roles that surface seal layer, microtopography, and vegetation play in the rainfall-infiltration-runoff process at the hillslope scale. For this purpose, we developed a model named Cell-based Rainfall-Infiltration-Runoff Model (CeRIRM). CeRIRM consists of two main modules: an infiltration model capable of accounting for soils with a seal layer (a two-layer profile), and a 2-D runoff routing model capable of addressing spatial dynamics of overland flow movement. The combined model can be used to study complex rainfall-infiltration-runoff processes in heterogeneous areas.

3.1. The Infiltration Model

[19] The two-layer infiltration model presented in Smith *et al.* [1993, 1999] and Corradini *et al.* [1994, 1997] was applied in this study. The governing equations in this model read

$$C_1(\psi_0) \frac{d\psi_0}{dt} = \frac{1}{\alpha_s Z_c} \left[i_0 - K_0 - \frac{K_{1s} G_1(\psi_c, \psi_0)}{Z_c} \right] \quad (6)$$

$$\begin{aligned} \frac{d\psi_c}{dt} = & \frac{1}{P(\psi_0, \psi_c, t)} \left\{ K_0 + \frac{K_{1s} G_1(\psi_c, \psi_0)}{Z_c} - K_{2c} \right. \\ & \left. - \frac{\beta_2(\theta_{2c}) p_2(\theta_{2c} - \theta_{2i}) K_{2s} G_2(\psi_i, \psi_c)}{I - Z_c[\theta_{1c} - \theta_{1i} + (\theta_0 - \theta_{1c})\alpha_s] - K_{2i}t} \right\} \end{aligned} \quad (7)$$

with the function $P(\psi_0, \psi_c, t)$ defined as

$$\begin{aligned} P(\psi_0, \psi_c, t) = & [\beta_2(\theta_{2c}) + \gamma_2(\theta_{2c} - \theta_{2i})] \cdot \\ & \left\{ \frac{I - Z_c[\theta_{1c} - \theta_{1i} + (\theta_0 - \theta_{1c})\alpha_s] - K_{2i}t}{(\theta_{2c} - \theta_{2i})\beta_2(\theta_{2c})} C_2(\psi_c) \right\} \\ & +(1 - \alpha_s) Z_c C_1(\psi_c) \end{aligned} \quad (8)$$

where t is time, Z_c is the seal layer thickness, ψ is capillary head, θ is water content, K is unsaturated soil hydraulic conductivity, and K_s is the saturated hydraulic conductivity, α_s is the weighting coefficient for surface wetting and interface wetting in the sealing layer, $C_1(\psi_0) = d\theta_0/d\psi$ is the slope of retention curve, G is the capillary drive defined as,

$$G(\psi_a, \psi_b) = \frac{1}{K_s} \int_{\psi_a}^{\psi_b} K(\psi) d\psi, \quad i_0 \text{ is the infiltration rate}$$

through soil surface, I is the cumulative infiltration, and γ , β , and p are coefficients related to the shape of the soil water content profile and are determined by relations presented in Corradini *et al.* [1997] and Smith *et al.* [1999]. The subscripts 1 and 2 denote quantities in the seal layer and the underlying soil, respectively; the subscripts 0 and c denote quantities at soil surface and seal layer-underlying soil interface, respectively; and the subscript i denotes quantities of initial conditions.

[20] Equations (6)–(8) describe the soil water movement in the top layer and underlying soil. The major advantage for using ψ instead of θ as the independent variable is that, unlike for θ , continuity in ψ holds at the interface between the seal layer and the undisturbed soil below [Smith *et al.*, 1999]. In addition, soil moisture redistribution is also included in equations (6)–(8) so that the model is applicable for rainstorms with multiple rainfall hiatuses. The model is driven by the rainfall as the surface boundary condition. It assumes a semi-infinite profile so that no bottom boundary condition is required. The two governing equations can be solved simultaneously to determine infiltration into the two-layer soil system. The model, which estimates appropriately the temporal evolution of θ at both the surface and the interface of the seal layer and the underlying soil, cannot provide detailed soil water content profiles; however, the infiltration rate it provides is adequate for this study. Last, in the areas where a seal layer is not present, the two-layer model reduces substantially to that proposed by Corradini *et al.* [1997] for homogeneous soil using a single ordinary differential equation.

3.2. The Overland Flow Model

[21] A 2-D diffusion wave model is applied in this study for runoff routing simulation. The governing equations read

$$\begin{cases} \frac{\partial H}{\partial t} + \frac{\partial q_x}{\partial x} + \frac{\partial q_y}{\partial y} = p_r - i_0 \\ S_0 - \frac{\partial h}{\partial s} = S_f \\ q = \frac{1}{n_f} h^3 S_f^2, \quad q_x = q \cos \alpha_f, \quad q_y = q \sin \alpha_f \end{cases} \quad (9)$$

where H is vertical flow depth, q_x and q_y are unit discharge in x and y directions, $q = \sqrt{q_x^2 + q_y^2}$ is the unit discharge in actual flow direction, p_r is rainfall intensity, i_0 is the infiltration rate same as the notation in equation (6), h is the flow depth normal to the slope, S_0 is the slope gradient, S_f is the friction slope, s is the flow direction, n_f is Manning's friction coefficient, α_f is the angle between s and x , and α_f can be determined by flow surface gradients in x and y coordinates. Similar equations using the kinematic wave approximation were adopted by Liu *et al.* [2004]. This approach applies the diffusion wave approximation to the actual flow direction, which is a direct generalization to the 1-D diffusion wave theory. It also preserves the hyperbolic form of the shallow water (full dynamic wave) flow equations so that numerical solutions developed for the shallow water flow equations are still applicable.

[22] Combining the governing equations (6)–(9), infiltration and runoff routing are both incorporated to describe the coupled process, where the infiltration rate is treated as a sink term. The 2-D approach allows representation of spatial variability of runoff and infiltration, so that surface features such as microtopography and vegetation patches can be addressed explicitly. With the 2-D approach, the run-on process in which runoff changes the water supply to downstream areas and increases loss to infiltration [e.g., Corradini *et al.*, 1998] can be naturally included in the model.

3.3. Numerical Approach for the Infiltration Module

[23] The two governing equations (6) and (7) for the infiltration model are two ordinary differential equations, therefore a standard Runge-Kutta fourth-order (RK4) approach is well suitable for seeking the numerical solution. The formulation of the RK4 approach for a set of ordinary differential equations can be found in references of numerical methods [e.g., Hoffman, 2001].

3.4. Numerical Approach for the Runoff Module

[24] The numerical approach for solving the 2-D diffusion wave equation is a finite volume, total variation diminishing (TVD)-MacCormack scheme proposed by Lin *et al.* [2003]. TVD schemes are a class of numerical schemes for parabolic partial differential equations that requires the total variation of the discrete solution not to increase. TVD schemes help preserve the monotonicity of the solution and eliminate nonphysical oscillations. Modern TVD schemes usually involve flux limiters to achieve TVD properties and high-order accuracy as well. Although originally developed for shock capturing in aerodynamics, TVD schemes have been widely applied in shallow water problems. Large amount of references of TVD schemes are available in the literature [e.g., Chung, 2002] and readers can refer to these references for more details.

[25] The Lin *et al.* [2003] scheme inherits the second-order accuracy of the well-known MacCormack scheme and carries the advantage of TVD schemes in suppressing nonphysical oscillation. Therefore, it is well suitable for shallow water flow problems. The approach is briefly explained below.

[26] Rewrite the shallow water flow equation in the vector form

$$\frac{\partial P}{\partial t} + \nabla \cdot \vec{F} = S \quad (10)$$

where P is the vector of the conserved variable, \vec{F} is the flux vector, and S is the source/sink term. In the full version of the shallow water equation, P and \vec{F} are matrices. Since in our model, the momentum equations are simplified with the diffusion wave approximation, here $P = H$ and $\vec{F} = q_x \vec{i} + q_y \vec{j}$. This equation can be integrated over a grid cell (i, j) as

$$\frac{\partial}{\partial t} \int P dA + \oint \vec{F} d\Gamma = \int S dA \quad (11)$$

where A is the area of the cell and Γ is the cell boundary. In this approach, the governing equation is solved using a prediction and a correction in each time step. In the time step $t = [t_n, t_{n+1}]$, discretized equations for cell (i, j) for prediction and correction, respectively, are

$$\hat{P}_{ij} = P_{ij}^n - \frac{\Delta t}{A} \left[\sum_{m=1}^8 F^{(1)}(\bar{P}) L^m \right]_{ij} + \Delta t S_{ij}^n \quad (12)$$

and

$$P_{ij}^{n+1} = P_{ij}^n - \frac{\Delta t}{A} \left[\sum_{m=1}^8 F^{(2)}(\bar{P}) L^m \right]_{ij} + \Delta t \hat{S}_{ij}^n \quad (13)$$

where \hat{P} is the predicted result of the conserved variable. The first-order numerical flux $F^{(1)}(\bar{P})$ through the cell boundary is calculated by

$$F^{(1)}(\bar{P}) = F_{LR} = F_L^+ + F_R^- \quad (14)$$

where F_L^+ and F_R^- are the left and the right split fluxes at each piece of the cell boundary. For this diffusion wave model, they can be directly calculated along the flux direction. The second-order numerical flux $F^{(2)}(\bar{P})$ through the interface $(i+1/2, j)$ between cells (i, j) and $(i+1, j)$ is estimated by adding the anti-diffusive term with the flux limiter function to F_{LR} :

$$F^{(2)}(\bar{P}) = F_{LR} + \frac{1}{2} [\varphi(r_{i+1/2,j}^+) w_{i+1/2,j}^+ - \varphi(r_{i+1/2,j}^-) w_{i+1/2,j}^-] \quad (15)$$

$$\varphi(r) = \frac{r + |r|}{1 + |r|} \quad (16)$$

$$r_{i+1/2,j}^+ = \frac{w_{i-1/2,j}^+}{w_{i+1/2,j}^+}; \quad r_{i+1/2,j}^- = \frac{w_{i+3/2,j}^-}{w_{i+1/2,j}^-} \quad (17)$$

$$w_{i+1/2,j}^+ = \hat{F}_{i+1,j}^- - F_{ij}^+; \quad w_{i+1/2,j}^- = F_{i+1,j}^- - \hat{F}_{ij}^- \quad (18)$$

where $\phi(r)$ is a flux limiter that introduces TVD properties into the numerical scheme. Flux at other cell interfaces can be derived similarly.

3.5. Mesh Configuration

[27] Mesh configuration is closely related to the implementation of the numerical scheme, thus critical for the entire approach. In general, an optimized computational

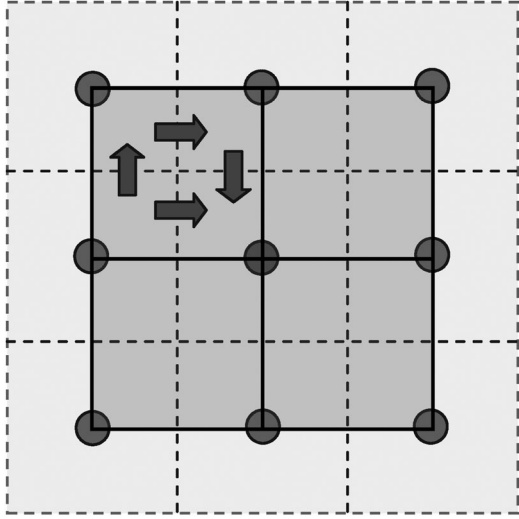


Figure 3. The structure of computational grid for runoff modeling. The dashed lines define mass cells in which calculation of mass balance (including infiltration) is conducted. Solid lines define dynamic cells in which the (simplified) momentum equations are computed. Each dynamic cell defines a topographic slope and a friction slope. The unit flow discharge q_x and q_y (shown in arrows) are also defined in dynamic cells.

grid can help suppress the numerical error generated during computation [Ferziger and Peric, 2002]. For overland flow simulation, it will also allow a simple treatment of topography, which is critical for simulating the shallow flow.

[28] In CeRIRM, the computational grid is consistent with the setting of common DEM data widely used in GIS environments so that handling topographic data is straightforward. As shown in Figure 3, elevation of the computation domain is defined at the cell center (node) of each grid cell (dashed-line squares), similar to the setting of a DEM grid. CeRIRM defines each grid cell as a mass cell in which mass balance computation is performed for both runoff and infiltration. Ground elevation z and water depth h are assigned for mass cells. Unit discharge components q_x and q_y are defined for the surrounding edges of a mass cell and are calculated within a dynamic cell (defined by solid lines in Figure 3). A dynamic cell is composed of four nodes. Computation of (simplified) momentum equations are implemented in dynamic cells. Topographic slope and friction slope are calculated in each dynamic cell using a bilinear function fitting for z and $z + h$ in this dynamic cell. Fluxes (unit discharge components q_x and q_y) can then be calculated in a dynamic cell using the slope value obtained in this cell. Such a staggered grid configuration is widely used in computational fluid dynamics. It is helpful to eliminate grid-induced unphysical oscillation usually seen in nonstaggered grids and is convenient for implementation of the numerical integration of the finite volume method in equations (11)–(13).

4. Characteristics of the Rainfall-Infiltration-Runoff Process

[29] The two main modules (infiltration and runoff routing) were validated separately by comparing with solutions

from other theoretical or widely accepted numerical models. The combined model was validated by comparing simulated results from two natural storm events to measured data (see Appendix A). The proposed model successfully simulated the rainfall-runoff process of the field plot in real semiarid environment, characterized by the presence of a seal layer at the bare soil surface, rockiness and vegetation patches, and topography. Therefore, it can be used to investigate the relative impact of each factor separately as well as their mutual interactions at that experimental plot. Several hypothetical cases were examined (Table 1): case (0)—a synthetic planar slope without the features of seal layer, microtopography and vegetation as reference; case (1)–case (0) plus a seal layer; case (2)–case (1) plus microtopography; case (3)–case (1) plus vegetation; case (4)–case (2) plus vegetation, which corresponds to simulating natural conditions at the plot. In the planar slope cases, we used a planar surface with the mean slope gradient of the natural plot. All cases accounted for the impact of the existing rock outcrop on infiltration. A natural storm event, Storm 1 (see section 2.1), that was considered in the validation phase, was used as the input. It is worth mentioning here that, in this storm, runoff began to generate when cumulative rainfall reached about 8 mm, much smaller than the total rainfall depth. This suggests that our study will be valuable also for storms with smaller rainfall depths.

4.1. Runoff Generation Mechanism

[30] Results of cumulative runoff generation curves are presented in Figure 4. Simulation result shows that no runoff was generated for case (0), the simple planar slope with the unsealed soil profile, and this case is not shown in Figure 4. Additional tests based on simulations of Storm 1 for the unsealed surface case, either with or without vegetation and with or without microtopography, did not generate runoff (hence results not shown), confirming the role of the seal layer in runoff generation. The seal layer was thus found to play a critical role in the hydrological response of LTER Lehavim site. When such a layer was absent, runoff could be generated only in cases of very high rainfall intensity events, which rarely occurred in the study area. Consequently, local water resources from rainfall under this condition will not be available to downstream areas through water redistribution by runoff. This implies that, in the case of unsealed soil surface, the water available for plants in this area will depend only on direct local rainfall input.

[31] The simulated results for case (1) (Figure 4) indicate that the seal layer formed on top of the undisturbed parent soil changed substantially the rainfall-runoff process in this area. When the seal layer is accounted for, runoff occurred due to the substantial reduction of soil permeability and related infiltration capacity. However, the simulated runoff under this condition was much higher than the observed value (22.6 mm versus 3.9 mm; see Appendix A), indicating that the seal layer is not the only factor controlling the rainfall-runoff response in this site.

[32] The effect of adding microtopography to the planar slope with a seal layer is depicted in case 2, Figure 4. The simulated runoff depth increased by a small amount (0.8 mm or 3.6%), indicating the microtopography is not a major factor controlling the total amount of runoff at the

Table 1. Hypothetical Cases Simulated for Runoff Mechanism Analysis

Case	Seal Layer	Microtopography	Vegetation	Note
Case 0	N ^a	N	N	A synthetic planar slope
Case 1	Y ^a	N	N	Case 0 plus a seal layer
Case 2	Y	Y	N	Case 1 plus microtopography
Case 3	Y	N	Y	Case 1 plus vegetation
Case 4	Y	Y	Y	Natural condition

^aN: feature not included; Y: feature included.

site. However, as will be presented later (section 4.2), microtopography changed the pattern of runoff routing, i.e., the overland flow movement, which could affect the amount of available water for local infiltration, and may have great impact on erosion (this aspect is not addressed in this study). The initiation of concentrated flow paths increased the flow routing speed. Thus, more water flowed out of the domain before being able to infiltrate into the soil, leading to the resulting increase in simulated runoff.

[33] The addition of the vegetation component to Case (1) resulted in a dramatic decrease of runoff depth (from 22.6 to 5.1 mm) (case 3, Figure 4), close to the observed value of 3.9 mm. This indicates that the combination between seal layer and vegetation patches is the main factor determining the total runoff depth in the site. Because of the large permeability of the soil below the shrubs, vegetation patches act as “sinks” that could capture a substantial part of the runoff generated in the sealed intershrubs areas. Ignoring the presence of the seal layer in the intershrubs areas, most rainfall would have infiltrated locally, therefore reducing drastically the water available for vegetation patches.

[34] Interestingly, accounting for microtopography reduced the simulated total runoff from the plot (comparing case (4) to case (2)). Because microtopography affected the spatial distribution of overland flow, it determines the specific contributing area to each vegetation patch. For the prescribed microtopography in the plot under interest, more water infiltrated into the vegetation patches, thus reducing the total runoff out of the plot. However, it is conceivable that a different microtopography could have led to an opposite result.

4.2. Spatial Pattern of Infiltration and Runoff

[35] Spatial distribution patterns of infiltration and runoff depth provide valuable information on the hydrological response. Figures 5 and 6 present the spatial distribution patterns of the cumulative infiltration (I) (Figure 5) and the combination between cumulative runoff (R_c) (positive values; Figure 6) and I (negative values; Figure 6) based on results for each cell, respectively. For Case (1) and Case (2) where vegetation was not included, I and R_c were relatively homogeneous across the plot surface (except in rock-covered areas). For the cases where vegetation was accounted for (cases 3 and 4), the respective spatial patterns of I and R_c were dramatically different. The pattern of I coincided with vegetation distribution, and showed a strong difference between upstream and downstream patches. Infiltration in vegetation patches was higher than in sealed intershrubs areas by one order of magnitude. In some areas, infiltration in vegetation patches was even higher than the total rainfall because of run-on contribution. However, upstream vegetation patches received less contri-

bution from run-on so that I in these areas is smaller compared to I in downstream patches. This prominent feature suggests that desert vegetation may receive much more water than local rainfall could provide, as a result of the multiplicative effect of the sealed areas that produce runoff accessible for the vegetation patches via overland flow. Spatial patterns of runoff generation (Figure 6) clearly illustrate that runoff was mainly produced in intershrub areas with the sealed soil surface. Large negative values (net infiltration) are simulated at vegetation patch locations, confirming the function of vegetation patches as water sinks. Microtopography imposed small changes to the infiltration distribution, indicating that its major effect is in shaping the spatial distribution of overland flow.

[36] To examine the spatial pattern of overland flow under different conditions, we analyzed the simulated flow depth and unit discharge results at the time of peak flow ($t = 29.83$ h) in Storm 1 for each case. Figures 7 and 8 show snapshots of flow depth and unit discharge distributions across the plot at the selected peak flow time. The flow depth and unit discharge contour lines are nearly straight horizontal lines on a planar slope with only sporadic rock coverage (Case 1 in Figures 7 and 8). With the appearance of microtopography, flow converged to depressions, forming concentrated flow paths (Case 2). Vegetation, wherever occurred, dramatically changed flow patterns regardless of microtopography (Cases 3 and 4). Overland flow was fully intercepted by vegetation patches

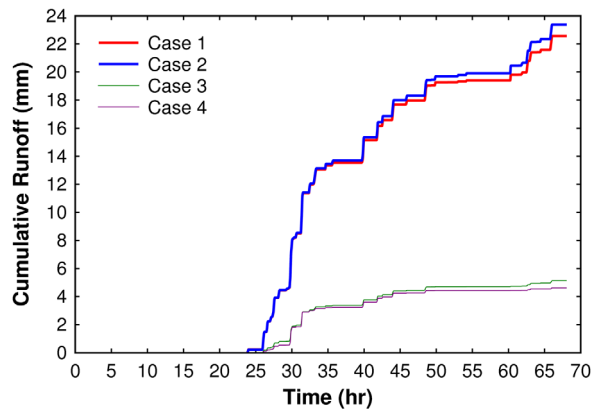


Figure 4. Simulated cumulative runoff under Storm 1. Case 1: A planar sloping plot with surface sealing layer; Case 2: A plot with microtopography and a seal layer but without vegetation; Case 3: A planar sloping plot with a seal layer and vegetation; and Case 4: A plot with microtopography, a seal layer and vegetation (i.e., the natural condition).

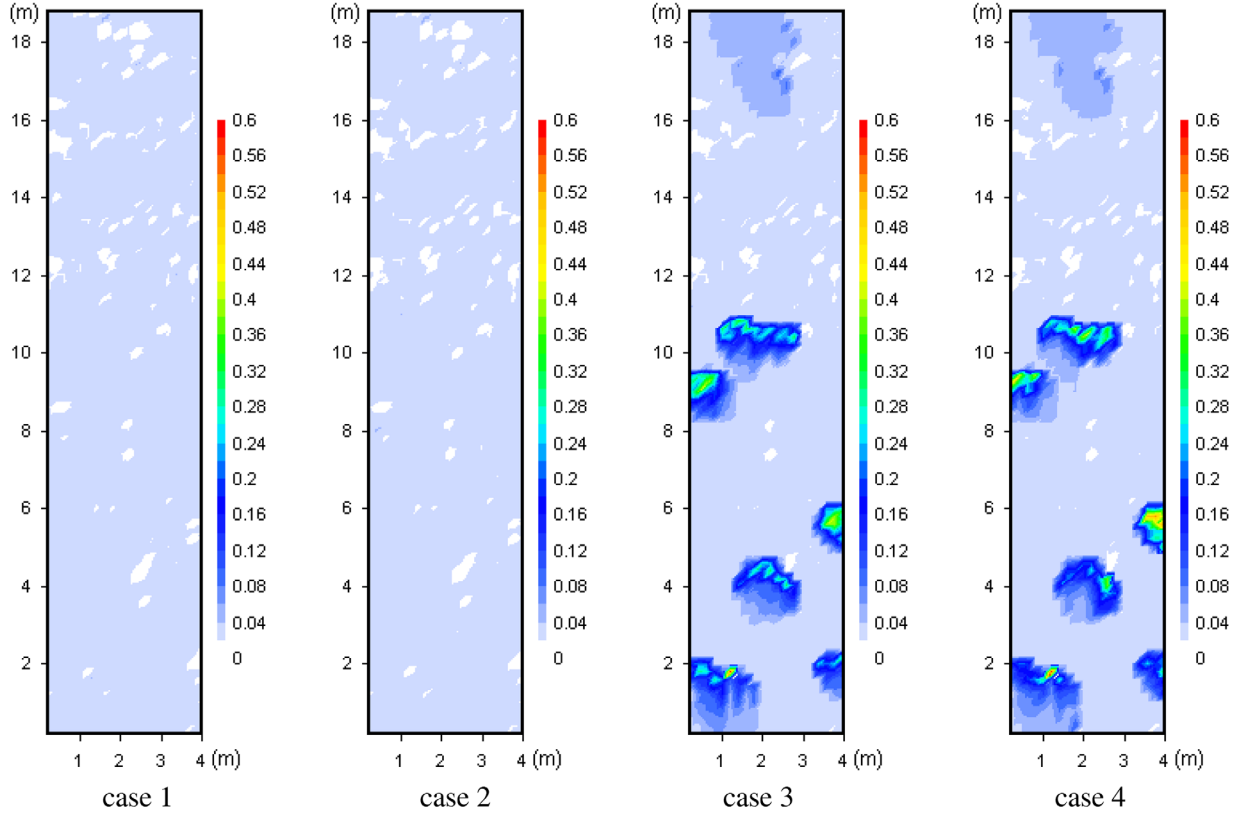


Figure 5. Spatial distribution of cumulative infiltration I (m). Configurations of cases are the same as described in Table 1 and caption of Figure 4.

in the upstream side of the plot where contributing areas to the patches were small and so was the flow; thus, all the supplied water could infiltrate. In downstream patches, flow depth was higher than in the surrounding intershrubs areas. This was mainly due to different surface roughness values between the two types of area. However, unit discharge at these patches was smaller than adjacent intershrubs areas, indicating a substantial part of the flow infiltrated. Comparing Cases (3) and (4) in both Figures 7 and 8, microtopography increased the flow depth and unit discharge at some patches while decreased them at others, depending on how microtopography diverted locally the overland flow. This suggests that microtopography may have opposite effects on runoff depth, depending on the specific local conditions.

[37] Microtopography may further complicate its impact through directly storing runoff on the surface. In our plot, surface storage is not important at the grid scale and was automatically included in the model. The subgrid surface storage was not accounted for due to lacking of hyper-resolution (10^{-2} to 10^{-3} m) data. Thompson *et al.* [2010a, 2010b] showed that this feature can significantly affect runoff and that such an effect was strongly dependent on slope. The effect of microtopography may be more complex than showed here and worth further studies.

5. Concluding Remarks

[38] The hydrological response of a complex natural system in a semiarid environment was analyzed. For given soil hydraulic properties and climatic data, the main factors iden-

tified to affect the hydrological responses were: topography including microtopography (surface roughness); the presence of a seal layer at the soil surface; rock outcrops; and vegetation patches. A model was developed to explicitly address these components and analyze their respective roles in shaping the integrated response. The model is composed of a two-layer infiltration module and a 2-D surface runoff routing module. It was successfully validated against field measured rainfall-runoff data in plots within the study area.

[39] Accounting for the surface seal layer is critical for runoff generation in the study area due to the relatively large permeability of the undisturbed soil and the usually short rainfall events. Without the effect of the seal layer on infiltration, no runoff could be generated in this area. Vegetation is another important factor affecting total runoff, since soil underneath it acts as a sink for runoff generated in sealed intershrub areas. The joint effect of these two components of the hydrological system largely determines the total runoff. Under the examined conditions, microtopography does not affect substantially the overall runoff generation process, but it can produce concentrated flow paths, altering the flow routing speed, the intensity of the run-on process, and eventually the amount of runoff. Microtopography also changes allocation of run-on to local areas, thus altering infiltration, and eventually water availability to local vegetation patches. The combined effect of the presence of a seal layer and microtopography increased available water resources up to an order of magnitude for downstream vegetation patches. This implies that these two components are crucial for the resilience of vegetation patches in dry environments, where water is a major limiting

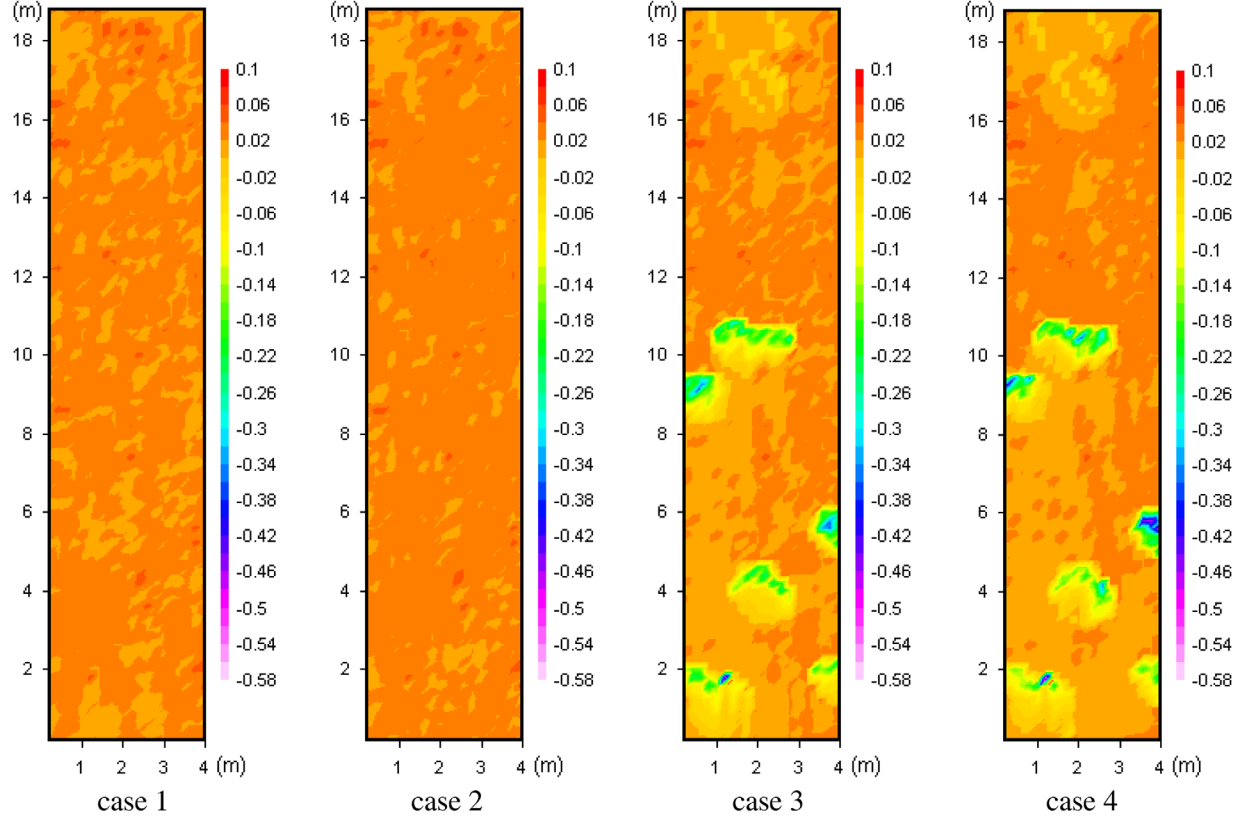


Figure 6. Spatial distribution of the combination between cumulative runoff R_c (positive values) and cumulative infiltration I (negative values) (m). Configurations of cases are the same as described in Table 1 and caption of Figure 4.

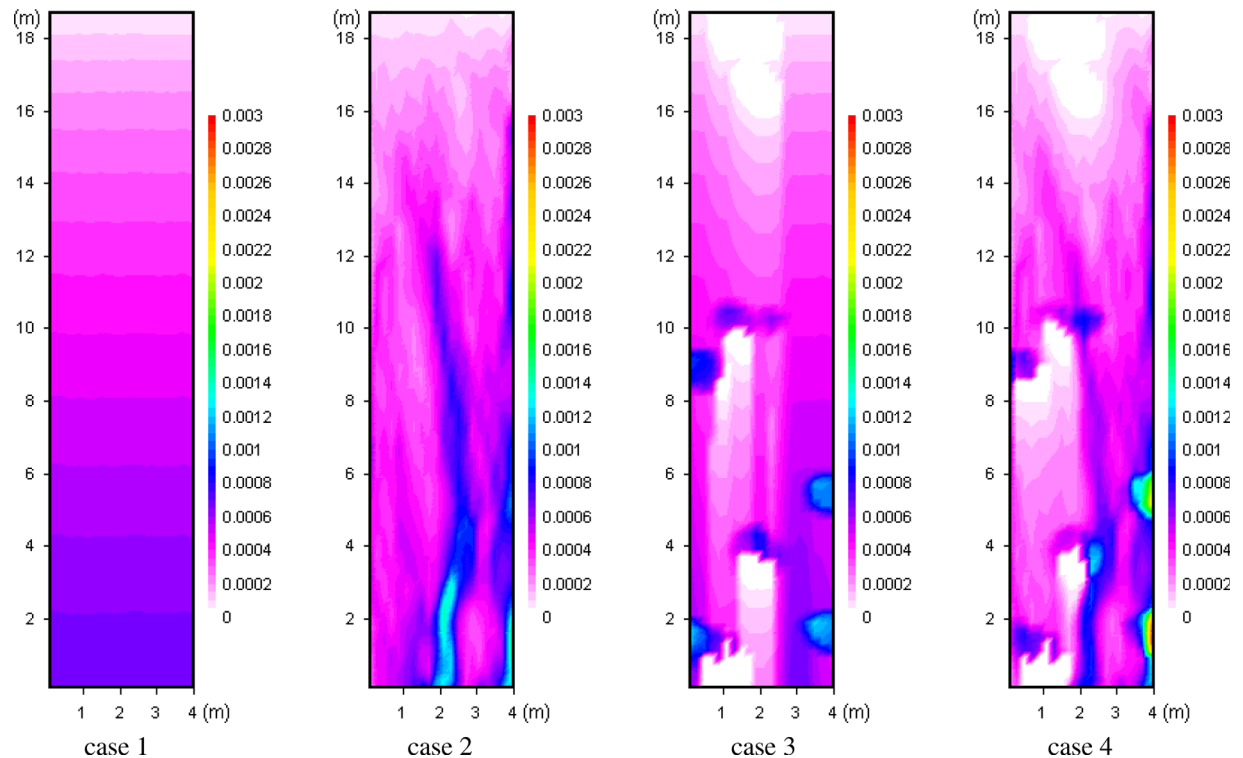


Figure 7. Spatial distribution of overland flow depth (m) at the time of peak flow ($t = 29.83$ h) in Storm 1. Configurations of cases are the same as described in Table 1 and caption of Figure 4.

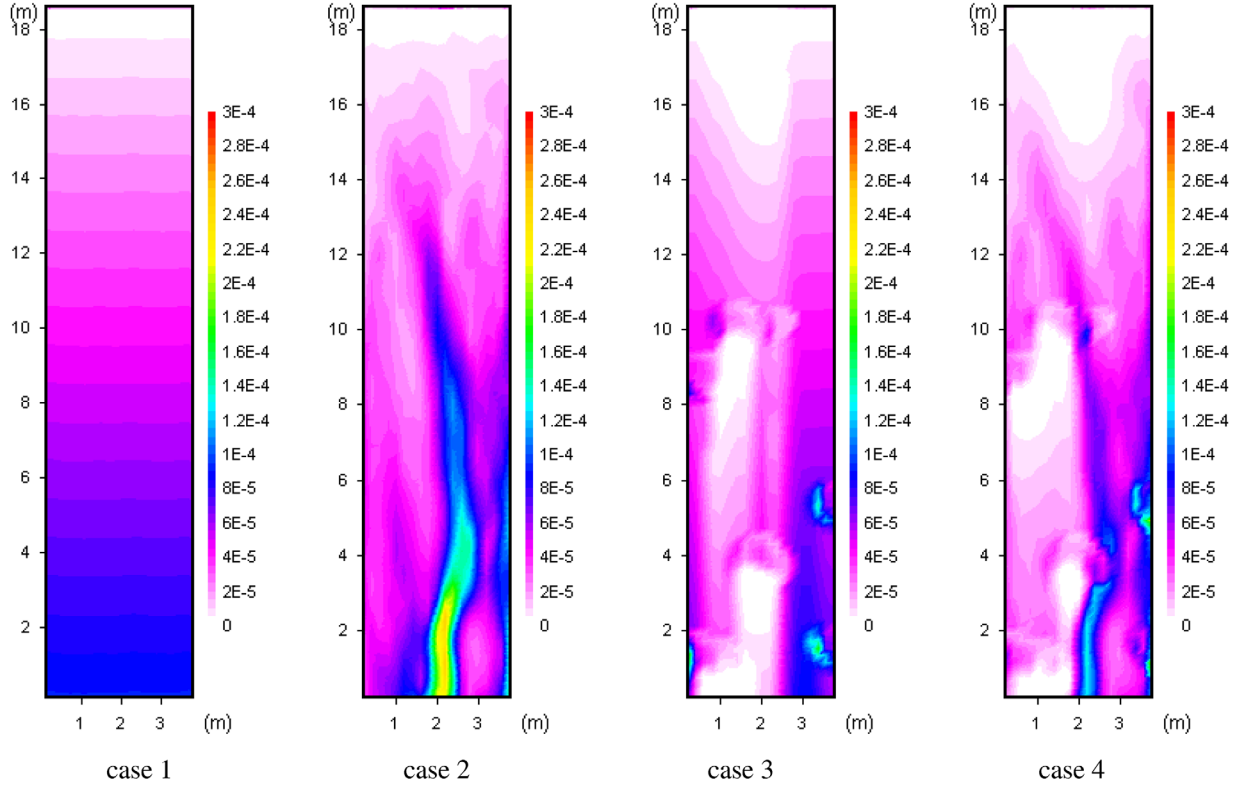


Figure 8. Spatial distribution of overland flow unit discharge ($\text{m}^2 \text{ s}^{-1}$) at the time of peak flow ($t=29.83 \text{ h}$) in Storm 1. Configurations of cases are the same as described in Table 1 and caption of Figure 4.

factor. Accounting for vegetation patches, the impact of microtopography was amplified under the conditions of the simulation. However, it is expected that microtopography may affect the system in different manners (either increasing or decreasing runoff as well as local water supply) and to different extents depending on the specific local conditions.

[40] Hydrological processes addressed in this study at a plot scale may behave differently at large scales. However, the model developed in this study can still be applied to large scales with high-resolution grid. It is our interest to investigate the dynamics at larger scales in future studies. Nevertheless, the results of this study shed some lights on the complex interactions between the physical characteristics of hillslopes in semiarid environments that shape their hydrological response. The seal layer developed at the surface of bare soils exposed to high kinetic energy rainfall was often demonstrated as a factor that reduces infiltration, increases runoff and erosion, and therefore induces a vicious cycle that accelerates desertification in semiarid areas [e.g., Lavee *et al.*, 1998]. In this study, it is shown that, on the contrary, the seal layer could act as a positive factor preventing desertification as it contributes to increase significantly the amount of water available to vegetation patches.

Appendix A: Model Validation

A1. Infiltration Module Validation

[41] The two-layer infiltration module in the proposed model was validated against Richards' equation using the

two natural storms (section 2.1). The Richards' equation solution was obtained using the widely accepted vadose zone simulation package Hydrus-1D [Simunek *et al.*, 2005]. The soil data used for the infiltration model validation corresponded to the field plot. Soil parameters for the seal layer and the underlying soil were obtained as described in section 2.2 and are summarized in Table A1. To solve Richards' equation, we used the van Genuchten [1980] soil parameters for both the seal and the undisturbed soil layers; while for the two-layer model, we used a set of empirical functions modified from the Brooks-Corey [Brooks and Corey, 1964] relations to represent the soil characteristics as follows:

$$\Theta = \frac{\theta - \theta_r}{\theta_s - \theta_r} = \left(\frac{\psi + \psi_B}{\psi_B} \right)^{-\lambda} \quad (\text{A1})$$

$$k(\psi) = \frac{K}{K_s} = \left(\frac{\psi + \psi_B}{\psi_B} \right)^{-\eta-r} \quad (\text{A2})$$

where Θ is the saturation, $k(\psi)$ is the relative conductivity at pressure ψ , ψ_B is the bubbling pressure, λ is the pore-size distribution-parameter, and $\eta = 2 + 3\lambda$. The parameter r is an empirical coefficient used to improve agreement with the unsaturated hydraulic conductivity function resulting from the van Genuchten model. A value of $r=3$ was chosen for this validation. Use of equations (A1) and (A2) is mainly for the convenience of numerical calculation, because an analytical expression for the integral of the

Table A1. Soil Hydraulic Parameters for the Seal Layer and the Underlying Soil^a

	van Genuchten			Empirical				
	K_s (cm h ⁻¹)	α_v (cm ⁻¹)	n	K_s (cm h ⁻¹)	λ	ψ_B (cm)	θ_s	θ_r
Seal layer	0.019	0.0078	1.43	0.019	0.263	76.4	0.450	0.0394
Underlying soil	3.38	0.0096	1.47	3.38	0.318	66.4	0.472	0.0378

^aFor symbols see text.

capillary drive G (section 3.1) is available for these expressions.

[42] For the simulation study, the prescribed thickness of the seal layer was set at 40 mm, following the calibration results reported by Mualem and Assouline [1989] when using infiltration data from Benyaminini [1981] for a soil similar to the one in our experimental site.

[43] To test the module for simulating infiltration under complex rainfall conditions, two natural storm events (see section 2.1) were used as input for this validation study. Figure A1 depicts these two storm events and the simulation results by the infiltration module and Hydrus-1D. The conceptual two-layer model satisfactorily simulates infiltration rate and cumulative infiltration for both events. Compared with the results of the more complex Richards' equation, the simulation errors for ultimate cumulative infiltration are 0.2% and 4.1% for storm 1 and storm 2, respectively. Therefore, the two-layer infiltration approach is reliable when appropriate soil hydraulic parameters are applied.

A2. Runoff Routing Module Validation—Analytical Solution

[44] The runoff modeling approach was validated by simulating a 1-D kinematic wave problem with an analytical solution. In this problem, rainfall generates runoff on an impervious surface so that infiltration is excluded. Parameters defining this problem include slope gradient $S_0 = 0.0005$, slope length $L = 400$ m, Manning's $n_f = 0.020$ sm^{-1/3}, rainfall intensity $p_r = 20$ mm h⁻¹, and rainfall duration $t_r = 200$ min. The total event duration t_f was 300 min. The analytical solution for this problem based on the kinematic wave theory was provided by Stephenson and Meadows [1986] and was applied in several studies for 2-D

modeling verification [Stephenson and Meadows, 1986; e.g., Gottardi and Venutelli, 1993].

[45] The analytical solution for the unit width discharge hydrograph reads as follows:

$$\begin{aligned} q &= \alpha_f(pt)^m \quad 0 \leq t \leq t_c \\ q &= \alpha_f(pt_c)^m t_c < t \leq t_r \\ q &= pL - pm\alpha_f^{1/m} q^{(m-1)/m} (t - t_r) t_r < t \leq t_f \end{aligned} \quad (\text{A3})$$

where t_c is the time of concentration (i.e., the time that the runoff hydrograph reaches the equilibrium condition), $t_c = (L/\alpha_f p^{m-1})^{1/m}$, $\alpha_f = S_0^{1/2}/n_f$, and $m = 5/3$.

[46] The validation results for the runoff module, when compared with the analytical solution, are presented in Figure A2. In general, the simulation result matches the analytical solution very well, except in the rising limb of the hydrograph near equilibrium. As indicated in previous studies [Woolhiser and Liggett, 1967; Singh, 1996], the analytical solution based on kinematic wave approximation is not accurate in this zone compared with the more accurate full dynamic wave and diffusion wave solutions. In addition, our result is close to the 2-D diffusion wave modeling result by Gottardi and Venutelli [1993] for the same problem. Therefore, our modeling result by the proposed approach is considered satisfactory for this testing problem.

A3. Validation of the Entire Model—Observed Runoff

[47] Measured rainfall-runoff data from plot 11A [Kossovsky, 1994] in the Lehavim LTER were used to test the model capability of simulating actual runoff generation processes. All major factors that may potentially affect infiltration or runoff routing dynamics in the testing plot were considered to achieve a more realistic description of plot 11A. A high-resolution grid of 20 cm cell size was

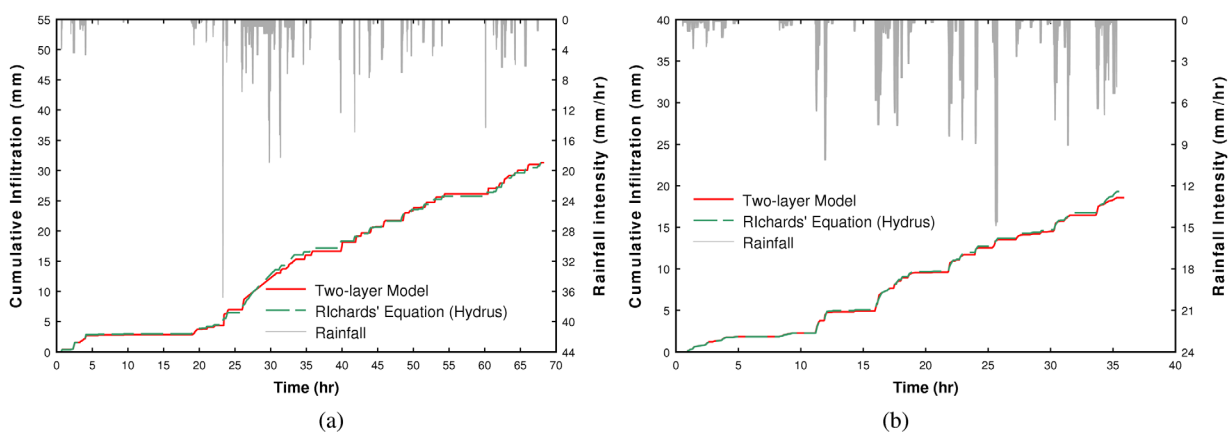


Figure A1. Validation for the two-layer infiltration module: (a) Storm 1 and (b) Storm 2.

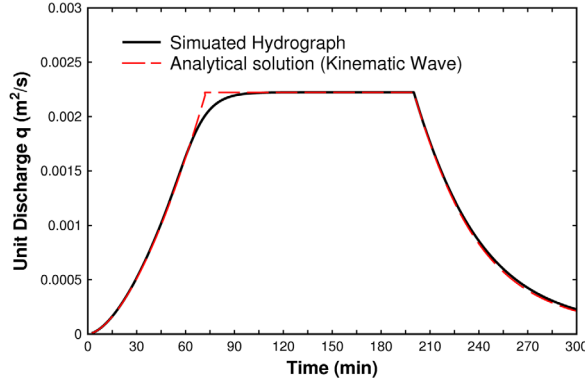


Figure A2. Comparison of simulated hydrograph and analytical solution for runoff generation on an impervious surface.

constructed, closely representing the complex topography using the interpolated elevation data (with a total of 1880 model cells). The mean slope of the 11A plot is 15%. Vegetation (dwarf shrub) distribution was mapped to the corresponding grid cells. The total vegetation coverage in the plot was about 13%, with more than half of these cells having a vegetation cover greater than 90%.

[48] For cells totally covered by vegetation, a single soil profile with no seal was applied in the infiltration model, and hydraulic conductivity corresponding to shrub-affected soil in the cell was used. For partially vegetated cells, a single-soil profile also was applied in the infiltration model, but area-averaged values of hydraulic conductivity combining the seal layer and shrub-affected soil in the cell were used. When cells represented completely bare soil, a two-layer soil profile was implemented in the infiltration model. The upper layer, representing the surface seal, was assigned the seal hydraulic properties as described above, and its thickness was set at 40 mm (see validation of infiltration module in section A1 of Appendix A). The hydraulic properties of the sealed layer and the underlying undisturbed soil are described in Table A1. Figure 2 shows the topogra-

phy, vegetation distribution, and top layer soil hydraulic conductivity distribution in the 11A plot.

[49] Since the rock outcrop is not negligible in this plot, we accounted for this effect in the model. After obtaining rock outcrop distribution in the plot as described in section 2.2, we mapped the percentage of rock area to each grid cell. When calculating infiltration, the portion of rock coverage was treated as an impervious surface and the percentage of rock area was applied as a reduction factor for each cell to obtain the actual infiltration amount. In the runoff module, different Manning's n_f values were used to distinguish vegetation-covered areas ($n_f = 0.1 \text{ m}^{-1/3} \text{ s}$) and inter-space areas ($n_f = 0.03 \text{ m}^{-1/3} \text{ s}$) [Singh, 1996]. Although rough estimate, this treatment provided a consistent and reproducible method to account for the impact of various surface features on flow resistance.

[50] Two runoff events for which observed rainfall and runoff data were available were chosen as the validation set. The two storms corresponding to these events, Storm 1 and Storm 2, are described in section 2.1 and presented in Figure A1. To apply more realistic initial water-content conditions in the soil prior to the onset of the storms used for model validations, relevant historic climate records of precipitation and evaporation values prior to these events in question were acquired from the Israel Meteorological Service. Using these climate records and the two-layer soil setting with van Genuchten soil hydraulic parameters, antecedent soil moisture conditions were estimated using the Hydrus-1D model [Simunek et al., 2005] by conducting a long-term soil moisture simulation from the beginning of the rainfall season (1 October) until a day before each validation storm event occurred. The Hydrus-1D modeling results were averaged for each layer and passed to the CeR-IRM model for rainfall-runoff simulation. The parameter r in equation (A2) for the unsaturated soil hydraulic conductivity function at the 11A plot was considered as a fitting parameter allowing accurate reproduction of the observed runoff. Using Storm 2 data, best fit between measured and simulated runoff was achieved for $r = 0.75$. This value was verified using Storm 1 data and was adopted in the simulations.

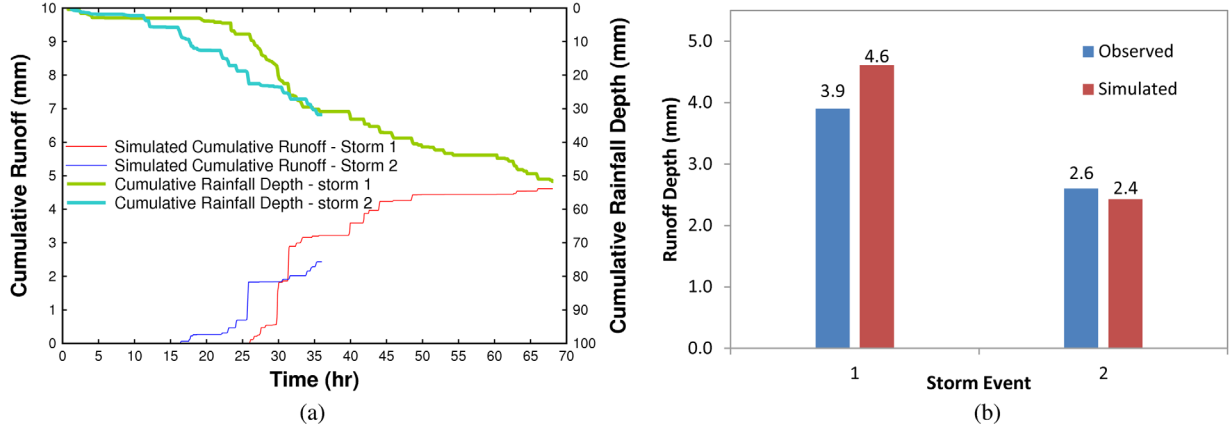


Figure A3. Simulated and observed runoff for the two storm events generated from the plot under examination: (a) time series of cumulative rainfall and simulated runoff and (b) simulated and observed runoff depth.

[51] Simulated results for the runoff depth resulting from the two storms are compared with field measurements in Figure A3, depicting that simulated total runoff is close to the observed value in both storm events. Considering the small runoff coefficient values measured in the field (7.6% and 8.2% for the storms 1 and 2, respectively), meaning that a small error in infiltration simulation can result in a larger error in runoff simulation, the simulation results indicated that the proposed model realistically simulates rainfall-runoff processes at the local scale.

[52] **Acknowledgments.** This study was funded by the International Arid Land Consortium (IALC) (grant 2010–34326-20783) and by the Israel Science Foundation (ISF) (grant 722 1184/11). The technical help of KfirNarkis from the Volcani Center and Or Livni from Ben-Gurion University is gratefully acknowledged. L. Chen particularly appreciates Michael H. Young in the Bureau of Economic Geology, University of Texas Austin for his generous help in the early stage of this study.

References

- Abrahams, A. D., A. J. Parsons, and J. Wainwright (1995), Effects of vegetation change on interrill runoff and erosion, Walnut Gulch, southern Arizona, *Geomorphology*, 13(1–4), 37–48, doi:10.1016/0169-555X(95)00027-3.
- Abu-Awwad, A. (1997), Water infiltration and redistribution within soils affected by a surface crust, *J. Arid Environ.*, 37(2), 231–242, doi:10.1006/jare.1997.0280.
- Ahuja, L. R. (1974), Applicability of the Green-Ampt approach to water infiltration through surface crust, *Soil Sci.*, 118(5), 283–288.
- Appels, W. M., P. W. Bogaart, and S. E. A. T. M. van der Zee (2011), Influence of spatial variations of microtopography and infiltration on surface runoff and field scale hydrological connectivity, *Adv. Water Resour.*, 34(2), 303–313, doi:10.1016/j.advwatres.2010.12.003.
- Assouline, S. (2002), Infiltration during soil sealing: The effect of areal heterogeneity of soil hydraulic properties, *Water Resour. Res.*, 38(12), 1286, doi:10.1029/2001WR001168.
- Assouline, S. (2004), Rainfall-induced soil surface sealing a critical review of observations, conceptual models, and solutions, *Vadose Zone J.*, 3(2), 570–591, doi:10.2113/3.2.570.
- Assouline, S. (2006), Modeling the relationship between soil bulk density and the hydraulic conductivity function, *Vadose Zone J.*, 5(2), 697–705, doi:10.2136/vzj2005.0084.
- Assouline, S. (2013), Infiltration into soils: Conceptual approaches and solutions, *Water Resour. Res.*, 49, 1755–1772, doi:10.1002/wrcr.20155.
- Assouline, S., and Y. Mualem (1997), Modeling the dynamics of seal formation and its effect on infiltration as related to soil and rainfall characteristics, *Water Resour. Res.*, 33(7), 1527–1536, doi:10.1029/96WR02674.
- Assouline, S., and Y. Mualem (2006), Runoff from heterogeneous small bare catchments during soil surface sealing, *Water Resour. Res.*, 42, W12405, doi:10.1029/2005WR004592.
- Belnap, J. (1990), Microbiotic crusts: Their role in past and present ecosystems, *Park Sci.*, 10(3), 3–4.
- Benyamin, Y. (1981), The behavior of bare soils under rainfall application, PhD thesis, Hebrew Univ. of Jerusalem, Jerusalem.
- Bhark, E. W., and E. E. Small (2003), Association between plant canopies and the spatial patterns of infiltration in shrubland and grassland of the Chihuahuan Desert, New Mexico, *Ecosystems*, 6(2), 185–196, doi:10.1007/s10021-002-0210-9.
- Bresler, E., and W. D. Kemper (1970), Soil water evaporation as affected by wetting methods and crust formation, *Soil Sci. Soc. Am. J.*, 34(1), 3–8, doi:10.2136/sssaj1970.03615995003400010008x.
- Bromley, J., J. Brouwer, A. P. Barker, S. R. Gaze, and C. Valentine (1997), The role of surface water redistribution in an area of patterned vegetation in a semi-arid environment, south-west Niger, *J. Hydrol.*, 198(1–4), 1–29, doi:10.1016/S0022-1694(96)03322-7.
- Brooks, R., and A. Corey (1964), *Hydraulic properties of porous media*, *Hydrology Papers*, Colorado State Univ., Fort Collins, CO.
- Caldwell, T. G., M. H. Young, J. Zhu, and E. V. McDonald (2008), Spatial structure of hydraulic properties from canopy to interspace in the Mojave Desert, *Geophys. Res. Lett.*, 35, L19406, doi:10.1029/2008GL035095.
- Cantón, Y., A. Solé-Benet, J. de Vente, C. Boix-Fayos, A. Calvo-Cases, C. Asensio, and J. Puigdefábregas (2011), A review of runoff generation and soil erosion across scales in semiarid south-eastern Spain, *J. Arid Environ.*, 75(12), 1254–1261, doi:10.1016/j.jaridenv.2011.03.004.
- Carmi, G., and P. Berliner (2008), The effect of soil crust on the generation of runoff on small plots in an arid environment, *Catena*, 74(1), 37–42, doi:10.1016/j.catena.2008.02.002.
- Chen, L., and M. H. Young (2006), Green-Ampt infiltration model for sloping surfaces, *Water Resour. Res.*, 42, W07420, doi:10.1029/2005WR004468.
- Chung, T. J. (2002), *Computational Fluid Dynamics*, Cambridge Univ. Press, Cambridge, UK.
- Corradini, C., F. Melone, and R. E. Smith (1994), Modeling infiltration during complex rainfall sequences, *Water Resour. Res.*, 30(10), 2777–2784, doi:10.1029/94WR00951.
- Corradini, C., F. Melone, and R. E. Smith (1997), A unified model for infiltration and redistribution during complex rainfall patterns, *J. Hydrol.*, 192(1–4), 104–124, doi:10.1016/S0022-1694(96)03110-1.
- Corradini, C., R. Morbidelli, and F. Melone (1998), On the interaction between infiltration and Hortonian runoff, *J. Hydrol.*, 204(1–4), 52–67, doi:10.1016/S0022-1694(97)00100-5.
- Davis, W. L., I. de Pater, and C. P. McKay (2010), Rain infiltration and crust formation in the extreme arid zone of the Atacama Desert, Chile, *Planet. Space Sci.*, 58(4), 616–622, doi:10.1016/j.pss.2009.08.011.
- Descoix, L., D. Viramontes, J. Estrada, J.-L. Gonzalez Barrios, and J. Asseline (2007), Investigating the spatial and temporal boundaries of Hortonian and Hewlettian runoff in Northern Mexico, *J. Hydrol.*, 346(3–4), 144–158, doi:10.1016/j.jhydrol.2007.09.009.
- Dunkerley, D. (2000), Hydrologic effects of dryland shrubs: Defining the spatial extent of modified soil water uptake rates at an Australian desert site, *J. Arid Environ.*, 45(2), 159–172, doi:10.1006/jare.2000.0636.
- Dunkerley, D. L. (2003), Determining friction coefficients for interrill flows: The significance of flow filaments and backwater effects, *Earth Surf. Processes Landforms*, 28(5), 475–491, doi:10.1002/esp.453.
- Dunkerley, D. (2004), Flow threads in surface run-off: Implications for the assessment of flow properties and friction coefficients in soil erosion and hydraulics investigations, *Earth Surf. Processes Landforms*, 29(8), 1011–1026, doi:10.1002/esp.1086.
- Dunne, T., W. Zhang, and B. F. Aubry (1991), Effects of rainfall, vegetation, and microtopography on infiltration and runoff, *Water Resour. Res.*, 27(9), 2271–2285, doi:10.1029/91WR01585.
- Erskine, R. H., T. R. Green, J. A. Ramirez, and L. H. MacDonald (2007), Digital elevation accuracy and grid cell size: Effects on estimated terrain attributes, *Soil Sci. Soc. Am. J.*, 71(4), 1371–1380, doi:10.2136/sssaj2005.0142.
- Essig, E. T., C. Corradini, R. Morbidelli, and R. S. Govindaraju (2009), Infiltration and deep flow over sloping surfaces: Comparison of numerical and experimental results, *J. Hydrol.*, 374(1–2), 30–42, doi:10.1016/j.jhydrol.2009.05.017.
- Ferziger, J. H., and M. Peric (2002), *Computational Methods for Fluid Dynamics*, 3rd ed., Springer, Berlin, Heidelberg, New York.
- Gottardi, G., and M. Venutelli (1993), A control-volume finite-element model for two-dimensional overland flow, *Adv. Water Resour.*, 16(5), 277–284, doi:10.1016/0309-1708(93)90019-C.
- Green, W. H., and G. A. Ampt (1911), Studies on soil physics, 1. The flow of air and water through soils, *J. Agric. Sci.*, 4(1), 1–24.
- Helmers, M. J., and D. E. Eisenhauer (2006), Overland flow modeling in a vegetative filter considering non-planar topography and spatial variability of soil hydraulic properties and vegetation density, *J. Hydrol.*, 328(1–2), 267–282, doi:10.1016/j.jhydrol.2005.12.026.
- Henkin, Z., N. G. Seligman, U. Kafkafi, and D. Prinz (1998), End-of-season soil water depletion in relation to growth of herbaceous vegetation in a sub-humid Mediterranean dwarf-shrub community on two contrasting soils, *Plant Soil*, 202(2), 317–326, doi:10.1023/A:1004370019120.
- Hillel, D., and W. R. Gardner (1969), Steady infiltration into crust-topped profiles, *Soil Sci.*, 108(2), 137–142.
- Hillel, D., and W. R. Gardner (1970), Transient infiltration into crust-topped profiles, *Soil Sci.*, 109(2), 69–76.
- Hoffman, J. D. (2001), *Numerical Methods for Engineers and Scientists*, Marcel Dekker, New York.
- Ivanov, V. Y., R. L. Bras, and E. R. Vivoni (2008a), Vegetation-hydrology dynamics in complex terrain of semiarid areas: 1. A mechanistic approach to modeling dynamic feedbacks, *Water Resour. Res.*, 44, W03429, doi:10.1029/2006WR005588.

- Ivanov, V. Y., R. L. Bras, and E. R. Vivoni (2008b), Vegetation-hydrology dynamics in complex terrain of semiarid areas: 2. Energy-water controls of vegetation spatiotemporal dynamics and topographic niches of favorability, *Water Resour. Res.*, 44, W03430, doi:10.1029/2006WR005595.
- Ivanov, V. Y., S. Fatichi, G. D. Jenerette, J. F. Espeleta, P. A. Troch, and T. E. Huxman (2010), Hysteresis of soil moisture spatial heterogeneity and the “homogenizing” effect of vegetation, *Water Resour. Res.*, 46, W09521, doi:10.1029/2009WR008611.
- Kidron, G. J., H. C. Monger, A. Vonshak, and W. Conrod (2012), Contrasting effects of microbiotic crusts on runoff in desert surfaces, *Geomorphology*, 139–140, 484–494, doi:10.1016/j.geomorph.2011.11.013.
- Kirkby, M. J., and R. J. Chorley (1967), Throughflow, overland flow and erosion, *Int. Assoc. Sci. Hydrol. Bull.*, 12(3), 5–21, doi:10.1080/0262666709493533.
- Kossovsky, A. (1994), Overland flow in a semi arid region, Lahav hills Israel, MSc thesis, Hebrew Univ. of Jerusalem, Jerusalem.
- Lange, J., and C. Leibundgut (2003), Surface runoff and sediment dynamics in arid and semi-arid regions, in *Understanding Water in a Dry Environment*, edited by I. Simmers, pp. 115–150, Taylor & Francis, Lisse, The Netherlands. [Available at <http://www.crcnetbase.com/doi/abs/10.1201/9780203971307.ch4>.]
- Lavee, H., A. C. Imeson, and P. Sarah (1998), The impact of climate change on geomorphology and desertification along a mediterranean-arid transect, *Land Degrad. Dev.*, 9(5), 407–422, doi:10.1002/(SICI)1099-145X(199809/10)9:5<407::AID-LDR302>3.0.CO;2-6.
- Lehmann, P., C. Hinz, G. McGrath, H. J. Tromp-van Meerveld, and J. J. McDonnell (2007), Rainfall threshold for hillslope outflow: An emergent property of flow pathway connectivity, *Hydrol. Earth Syst. Sci.*, 11(2), 1047–1063, doi:10.5194/hess-11-1047-2007.
- Lin, G.-F., J.-S. Lai, and W.-D. Guo (2003), Finite-volume component-wise TVD schemes for 2D shallow water equations, *Adv. Water Resour.*, 26(8), 861–873, doi:10.1016/S0309-1708(03)00075-7.
- Liu, Q., L. Chen, J. Li, and V. Singh (2004), Two-dimensional kinematic wave model of overland-flow, *J. Hydrol.*, 291(1–2), 28–41, doi:10.1016/j.jhydrol.2003.12.023.
- Mayor, Á. G., S. Bautista, E. E. Small, M. Dixon, and J. Bellot (2008), Measurement of the connectivity of runoff source areas as determined by vegetation pattern and topography: A tool for assessing potential water and soil losses in drylands, *Water Resour. Res.*, 44, W10423, doi:10.1029/2007WR006367.
- Mualem, Y., and S. Assouline (1989), Modeling soil seal as a nonuniform layer, *Water Resour. Res.*, 25(10), 2101–2108, doi:10.1029/WR025i010p02101.
- Mualem, Y., S. Assouline, and D. Eltahan (1993), Effect of rainfall-induced soil seals on soil water regime: Wetting processes, *Water Resour. Res.*, 29(6), 1651–1659, doi:10.1029/93WR00096.
- Muñoz-Robles, C., N. Reid, M. Tighe, S. V. Briggs, and B. Wilson (2011), Soil hydrological and erosional responses in patches and inter-patches in vegetation states in semi-arid Australia, *Geoderma*, 160(3–4), 524–534, doi:10.1016/j.geoderma.2010.10.024.
- Peel, M. C. (2009), Hydrology: Catchment vegetation and runoff, *Prog. Phys. Geogr.*, 33(6), 837–844, doi:10.1177/030913309350122.
- Philip, J. R. (1957), The theory of Infiltration: 1. The infiltration equation and its solution, *Soil Sci.*, 83(5), 345–358.
- Philip, J. R. (1991), Infiltration and downslope unsaturated flows in concave and convex topographies, *Water Resour. Res.*, 27(6), 1041–1048, doi:10.1029/91WR00129.
- Reid, K. D., B. P. Wilcox, D. D. Breshears, and L. MacDonald (1999), Runoff and erosion in a Piñon-Juniper woodland influence of vegetation patches, *Soil Sci. Soc. Am. J.*, 63(6), 1869–1879, doi:10.2136/sssaj1999.6361869x.
- Ribolzi, O., J. Patin, L. M. Bresson, K. O. Latsachack, E. Mouche, O. Sengtaheuanghong, N. Silvera, J. P. Thiébaux, and C. Valentin (2011), Impact of slope gradient on soil surface features and infiltration on steep slopes in northern Laos, *Geomorphology*, 127(1–2), 53–63, doi:10.1016/j.geomorph.2010.12.004.
- Römkens, M. J. M., R. L. Baumhardt, M. B. Parlange, F. D. Whisler, J. Y. Parlange, and S. N. Prasad (1986), Rain-induced surface seals: Their effect on ponding and infiltration in, *Ann. Geophys., Ser. B*, 4, 417–424.
- Saxton, K. E., W. J. Rawls, J. S. Romberger, and R. I. Papendick (1986), Estimating generalized soil-water characteristics from texture, *Soil Sci. Soc. Am. J.*, 50(4), 1031–1036, doi:10.2136/sssaj1986.0361599500500040039x.
- Segoli, M., E. D. Ungar, and M. Shachak (2008), Shrubs enhance resilience of a semi-arid ecosystem by engineering and regrowth, *Ecohydrology*, 1(4), 330–339, doi:10.1002/eco.21.
- Sela, S., T. Svoray, and S. Assouline (2012), Soil water content variability at the hillslope scale: Impact of surface sealing, *Water Resour. Res.*, 48(3), W03522, doi:10.1029/2011WR011297.
- Seneviratne, S. I., T. Corti, E. L. Davin, M. Hirschi, E. B. Jaeger, I. Lehner, B. Orlowsky, and A. J. Teuling (2010), Investigating soil moisture–climate interactions in a changing climate: A review, *Earth Sci. Rev.*, 99(3–4), 125–161, doi:10.1016/j.earscirev.2010.02.004.
- Simunek, J., M. Sejna, and M. T. van Genuchten (2005), The HYDRUS-1D software package for simulating the one-dimensional movement of water, heat, and multiple solutes in variably-saturated media, *Res. Rep.*, 240, Univ. of California, Riverside, Calif.
- Singh, V. P. (1996), *Kinematic Wave Modeling in Water Resources: Surface-Water Hydrology*, Wiley-Interscience, New York.
- Smith, R. E., and J.-Y. Parlange (1978), A parameter-efficient hydrologic infiltration model, *Water Resour. Res.*, 14(3), 533–538, doi:10.1029/WR014i003p00533.
- Smith, R. E., C. Corradini, and F. Melone (1993), Modeling infiltration for multistorm runoff events, *Water Resour. Res.*, 29(1), 133–144, doi:10.1029/92WR02093.
- Smith, R. E., C. Corradini, and F. Melone (1999), A conceptual model for infiltration and redistribution in crusted soils, *Water Resour. Res.*, 35(5), 1385–1393, doi:10.1029/1998WR900046.
- Stephenson, D., and M. E. Meadows (1986), *Kinematic Hydrology and Modelling*, Elsevier, Amsterdam and New York.
- Svoray, T., and A. Karnieli (2011), Rainfall, topography and primary production relationships in a semiarid ecosystem, *Ecohydrology*, 4(1), 56–66, doi:10.1002/eco.123.
- Svoray, T., R. Shafran-Nathan, Z. Henkin, and A. Perevolotsky (2008), Spatially and temporally explicit modeling of conditions for primary production of annuals in dry environments, *Ecol. Model.*, 218(3–4), 339–353, doi:10.1016/j.ecolmodel.2008.07.029.
- Tayfur, G., M. L. Kavvas, R. S. Govindaraju, and D. E. Storm (1993), Applicability of St. Venant equations for two-dimensional overland flows over rough infiltrating surfaces, *J. Hydraul. Eng.*, 119(1), 51–63, doi:10.1016/(ASCE)0733-9429(1993)119:1(51).
- Thompson, S. E., G. G. Katul, and A. Porporato (2010a), Role of microtopography in rainfall-runoff partitioning: An analysis using idealized geometry, *Water Resour. Res.*, 46(7), W07520, doi:10.1029/2009WR008835.
- Thompson, S. E., C. J. Harman, P. Heine, and G. G. Katul (2010b), Vegetation-infiltration relationships across climatic and soil type gradients, *J. Geophys. Res.*, 115, G02023, doi:10.1029/2009JG001134.
- Titus, J. H., R. S. Nowak, and S. D. Smith (2002), Soil resource heterogeneity in the Mojave Desert, *J. Arid Environ.*, 52(3), 269–292, doi:10.1006/jare.2002.1010.
- van Genuchten, M. T. (1980), A closed-form equation for predicting the hydraulic conductivity of unsaturated soils, *Soil Sci. Soc. Am. J.*, 44(5), 892–898, doi:10.2136/sssaj1980.03615995004400050002x.
- Vandervaere, J. P., M. Vauclin, R. Haverkamp, C. Peugeot, J. L. Thony, and M. Gilfedder (1998), Prediction of crust-induced surface runoff with disc infiltrometer data, *Soil Sci.*, 163(1), 9–21.
- Wainwright, J., and L. J. Bracken (2011), Runoff generation, overland flow and erosion on hillslopes, in *Arid Zone Geomorphology*, edited by D. S. G. Thomas, pp. 235–267, John Wiley.
- Woolhiser, D. A., and J. A. Liggett (1967), Unsteady, one-dimensional flow over a plane—The rising hydrograph, *Water Resour. Res.*, 3, 753–771, doi:10.1029/WR003i003p00753.
- Yair, A., and A. Kossovsky (2002), Climate and surface properties: hydrological response of small arid and semi-arid watersheds, *Geomorphology*, 42(1–2), 43–57, doi:10.1016/S0169-555X(01)00072-1.
- Zaslavsky, D., and G. Sinai (1981), Surface hydrology: I—Explanation of Phenomena, *J. Hydraul. Div.*, 107(1), 1–16.
- Zhang, W., and T. W. Cundy (1989), Modeling of two-dimensional overland flow, *Water Resour. Res.*, 25(9), 2019–2035, doi:10.1029/WR025i009p02019.
- Zhang, W., and D. R. Montgomery (1994), Digital elevation model grid size, landscape representation, and hydrologic simulations, *Water Resour. Res.*, 30(4), 1019–1028, doi:10.1029/93WR03553.